Research Article

Personalized Facial Wrinkle Distribution Analysis Using Backpropagation Neural Network (BPNN)

[1] Magfiratul Jannah, [2,*]Desi Anggreani, [3]Muhyiddin A. M Hayat

[1,2,3] Department of Informatics Engineering, Universitas Muhammadiyah Makassar, South Sulawesi, Indonesia

* Corresponding Author: desianggreani@unismuh.ac.id

Abstract: Facial wrinkle distribution is an important indicator of aging and lifestyle. This study proposes a personalized wrinkle classification system using a Backpropagation Neural Network (BPNN) based on segmented facial areas such as the forehead, eyes, cheeks, and mouth. After preprocessing and feature extraction, the BPNN model is trained to classify wrinkle severity into two categories: high and medium. Evaluation results show that the model performs well, particularly in detecting the Medium class, achieving a precision of 0.8438 and a recall of 0.9310, while for the High class, the precision is 0.8333 and the recall is 0.6667. These findings indicate that the BPNN architecture is effective and reliable in facial wrinkle classification, with potential applications in dermatology, cosmetic analysis, and digital forensics.

Keywords: facial wrinkles, backpropagation neural network, image segmentation, aging analysis, artificial intelligence, deep learning.

Citation: Magfiratul Jannah, M., Anggreani, D., & Hayat, M. A. M. (2025). Personalized facial wrinkle distribution analysis using backpropagation neural network (BPNN). *Iota*, 5(3). https://doi.org/10.31763/iota.v5i3.1000

Academic Editor: Adi, P.D.P

Received: June 21, 2025

Accepted: July 12, 2025

Published: August 01, 2025

Publisher's Note: ASCEE stays neutral about jurisdictional claims in published maps and institutional affiliations.

1. Introduction

Skin aging is a biological process influenced by intrinsic and extrinsic factors, where wrinkles act as visible indicators of aging [1]. Accurate wrinkle analysis plays an important role in medical diagnostics, cosmetic product development, and forensic investigations [2]. However, traditional wrinkle detection methods are often limited in handling nonlinear patterns and subtle micro-texture variations [3].

Recent advances in deep learning techniques have significantly improved the performance of wrinkle detection. Moon et al. introduced FFHQ-Wrinkle, a large annotated dataset with texture map-based weak supervision, which achieved notable segmentation accuracy [4]. Kim et al. developed a U-Net model with weighted deep supervision and semi-automatic labeling to enhance wrinkle boundary precision [5]. Similarly, Zhang et al. proposed a novel CNN-based approach with a distance-based loss function to improve fine wrinkle detection [6]. These studies have shown strong results but often require large datasets and high computational resources, limiting their feasibility for lightweight or real-time applications [7].

In this study, we propose a Backpropagation Neural Network (BPNN) with region-based facial segmentation for wrinkle detection. The proposed method combines texture and contour features extracted from key facial regions and applies a computationally efficient neural network architecture [8]. This approach aims to achieve competitive accuracy while maintaining low computational cost, making it suitable for small datasets and practical deployments [9].

2. Theory

Aging is a complex biological process that affects all human organs, including the skin. The skin, especially the facial area, is the most visible part of aging due to the appearance of wrinkles, loss of elasticity, and structural degradation. These visible signs are influenced by a combination of genetic, environmental, and lifestyle factors. To understand and analyze the distribution of facial wrinkles accurately, it is essential to

explore the theoretical foundations behind skin aging, digital image processing, and neural network modeling. This section outlines the relevant theories that underpin the methodology used in this study.

2.1 Skin Aging and Wrinkle Formation

Aging is a complex biological process that affects all human organs, especially the skin. Wrinkle formation results from the breakdown of collagen and elastin fibers due to intrinsic factors such as genetics and hormonal changes, as well as extrinsic factors including UV radiation, environmental pollution, smoking, and inadequate skincare [10]. These factors increase free radical production and activate matrix metalloproteinase enzymes, accelerating dermal degradation and leading to reduced elasticity, dryness, and deeper wrinkles [11].

2.2 Digital Image and Image Processing

Digital image processing enables wrinkle detection by enhancing and analyzing visual features from facial images [12]. Common preprocessing steps include grayscale conversion, resizing, and segmentation into specific regions (forehead, eyes, cheeks, and mouth) [13]. Recent studies have improved segmentation accuracy using U-Net with attention mechanisms [14], texture map-based weak supervision [4], and hybrid feature fusion techniques [15]. Such preprocessing enhances the performance of downstream feature extraction methods like the Gray Level Co-occurrence Matrix (GLCM) for texture analysis and Canny edge detection for contour analysis [16].

2.3 Wrinkle Detection Process

Wrinkle detection involves locating wrinkle-prone areas and extracting relevant features for classification. Traditional methods rely on texture filters such as Gabor filters and Hessian-based edge detection, while modern approaches incorporate deep learning architectures, including CNNs and attention-enhanced U-Nets [17] [18]. However, high-performing deep learning models often require substantial computational power and annotated data, which is not always feasible in resource-constrained environments [19].

2.4 Deep Learning

Deep learning models learn hierarchical features from raw data, making them suitable for tasks like wrinkle detection [20]. In particular, convolutional architectures excel at extracting local patterns, while fully connected networks like BPNN can be effective for small, well-engineered feature sets [21].

2.5 Backpropagation Neural Network (BPNN)

A Backpropagation Neural Network (BPNN) consists of an input layer, one or more hidden layers, and an output layer. In this study, the input layer represents the extracted features (texture and contour), while the hidden layers process nonlinear combinations using the Rectified Linear Unit (ReLU) activation function as the Equation 1.

$$f_{\mathrm{ReLU}}(x) \;=\; max\;(0, x) \tag{1}$$

The output layer applies the softmax function for multi-class classification as equation 2.

$$\sigma(z_i) = \frac{e^{z_i}}{\sum_j e^{z_j}} \tag{2}$$

The forward propagation process computes the net input for each neuron as equation 3.

$$z_j = \sum_i w_{ij} x_i + b_j \tag{3}$$

And the neuron output after activation as equation 4.

$$a_j = f(z_j) \tag{4}$$

The training objective is to minimize the cross-entropy loss between the predicted probability $\hat{y}_i$ and the true label y_i as the equation 5.

$$E = - \sum_{i-1}^{n} y_i \, log \, (\hat{y}_i) \tag{5}$$

The backpropagation process in BPNN consists of several key stages. First is the forward pass, where input features propagate through the network layer by layer. Each neuron computes a weighted sum of its inputs, adds a bias term, and applies the ReLU activation function. The output layer then applies Softmax to produce class probabilities. Second is the loss calculation, where the predicted probabilities are compared with the ground truth labels using the cross-entropy loss function (Equation 5). Third is the backward pass, where the error at the output layer is calculated and propagated backward through the network using the chain rule, allowing the calculation of gradients for each weight. Fourth is the gradient computation, which determines how much each weight contributed to the error. Finally, in the weight update stage, weights are adjusted according to the gradient descent rule in equation 6.

$$w_{ij}(t + 1) = w_{ij}(t) - \eta \times \frac{\partial E}{\partial w_{ij}} \tag{6}$$

Where η represents the learning rate. This iterative process repeats for several epochs until the model converges to an optimal solution. Figure X shows the overall BPNN workflow used in this study, while Figure Y illustrates the detailed step-by-step backpropagation process [22][23].

2.6 Evaluation Metrics

A Confusion Matrix is a key evaluation tool in classification tasks, offering detailed insights beyond overall accuracy, particularly in multi-class or imbalanced data [24]. It records prediction results as true positive (TP), true negative (TN), false positive (FP), and false negative (FN), which are then used to compute performance metrics [25]. Accuracy reflects the ratio of correct predictions in equation 7.

$$Accuracy = \frac{TP+TN}{TP+TN+FP+FN} \tag{7}$$

Precision measures the proportion of correctly predicted positives in equation 8.

$$Precision = \frac{TP}{TP+FP} \tag{8}$$

Recall shows the model's ability to detect actual positives in equation 9.

$$Recall = \frac{TP}{TP+FN} \tag{9}$$

F1-Score balances precision and recall in equation 10.

$$F1 - Score = 2 \times \frac{Precision \times Recall}{Precision + Recall} \tag{10}$$

These metrics are essential for evaluating the performance of BPNN in detecting facial wrinkles across segmented areas like the forehead, eyes, cheeks, and mouth, which present complex and varied patterns [26].

3. Method

This study was conducted from April to July 2025 in Makassar, primarily at Universitas Muhammadiyah Makassar, with data collected from several locations across the city. The research aims to classify facial wrinkle distribution based on segmented facial areas using a Backpropagation Neural Network (BPNN). A combination of image preprocessing, feature extraction, model training, and evaluation metrics was used to ensure effective classification results.

3.1 Data Collection and Preprocessing

The dataset used in this study consists of 800 facial images collected from local participants between April and July 2025 in Makassar, Indonesia, comprising two wrinkle severity classes: medium wrinkles (400 images) and high wrinkles (400 images). Data collection was conducted under controlled lighting and front-facing orientation to minimize shadows and distortions [27]. This dataset was selected due to its diversity in age, ethnicity, and skin condition, enabling the model to generalize effectively for personalized wrinkle detection.

All images were converted to grayscale to reduce computational complexity and resized to 200×200 pixels for uniformity [28]. The face was segmented into four distinct regions—forehead, eyes, cheeks, and mouth—using manual cropping guided by facial landmark detection algorithms [29]. For each region, texture features were extracted using the Gray Level Co-occurrence Matrix (GLCM) with three distances ($d = 1, 2, 3$) and four angles ($\theta = 0°, 45°, 90°, 135°$) [30]. Contour features, including the number of contours and total contour length, were obtained via Canny edge detection with adaptive thresholds [31].

3.2 Wrinkle Categorization

Wrinkle severity labeling was performed before model training to ensure consistent classification targets across all facial regions. For each segmented region (forehead, eyes, cheeks, and mouth), wrinkle features were statistically analyzed to determine threshold values [32]. Samples with feature values between the 50^{th} and 75^{th} percentiles were labeled as medium severity, while those above the 75^{th} percentile were labeled as high severity. This region-specific categorization approach accounts for the natural variation in wrinkle patterns across different facial areas [33], reducing bias and improving the model's ability to generalize.

3.3 Dataset Formation and Augmentation

Extracted features were compiled into a structured dataset with each row representing a single image and its six corresponding numerical features (three texture-based and three contour-based) [34]. Data augmentation was implemented by slightly perturbing feature values within ±5% to balance class distribution without introducing unrealistic samples [35]. All features were normalized using Min-Max scaling to the range [0, 1] before model training [36].

3.4 Model Architecture

A Multilayer Perceptron (MLP) architecture was implemented with one input layer, two hidden layers, and one output layer. The input layer consisted of six neurons corresponding to the extracted features, while the hidden layers contained 16 and 8 neurons, respectively, activated using ReLU functions. The output layer applied softmax activation for multi-class classification [37]. The flowchart system is shown in Figure 1, and the BPNN architecture is illustrated in Figure 2.

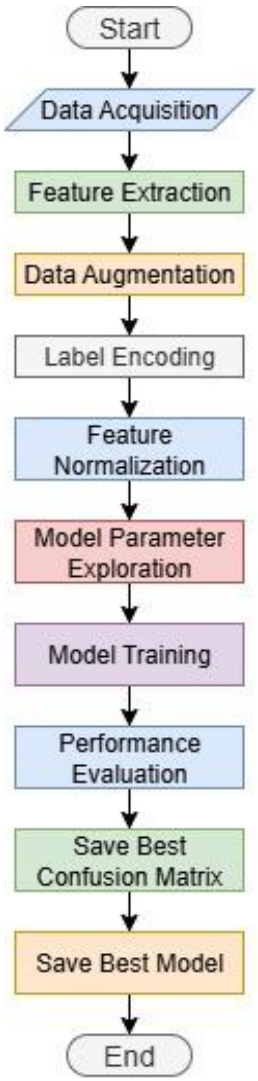

Figure 1. Flowchart System

The model was optimized through comparative experiments using different hidden layer configurations, including (8,8), (16,8), and (16,16), where the numbers indicate the neurons in the first and second hidden layers. The (16,8) configuration achieved the highest accuracy, balancing complexity and generalization. During training, the network applied the cross-entropy loss function (as described in Section 2) and updated weights using stochastic gradient descent through the backpropagation process [38][39].

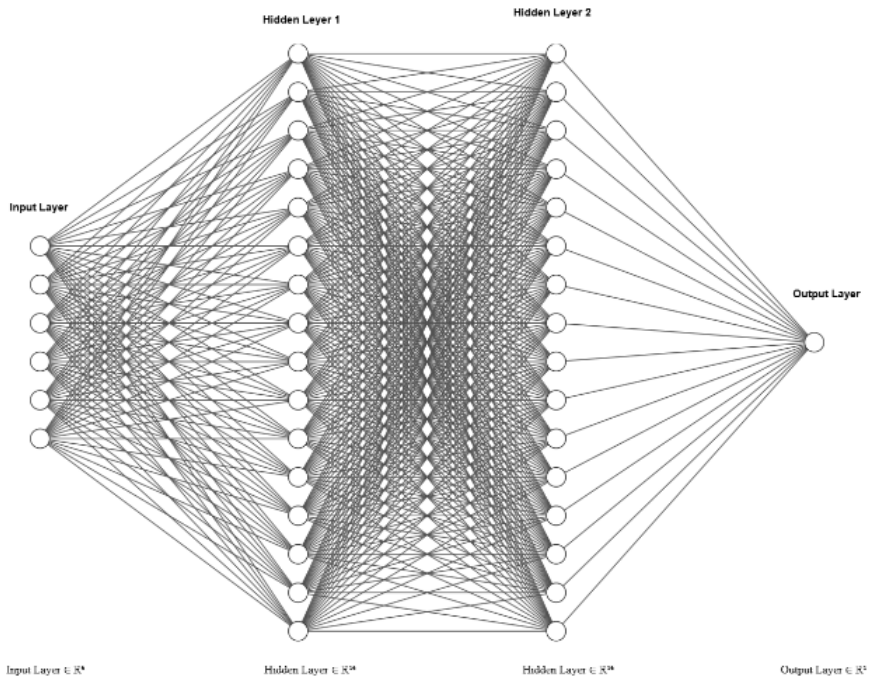

Figure 2. BPNN Model Architecture

3.5 Model Training

The training process included forward propagation for prediction and backward propagation for weight adjustment. Repeated iterations continued until the loss value stabilized. The training was validated using a portion of the dataset reserved for testing to ensure generalizability and prevent overfitting [40]. Model weights were updated using stochastic gradient descent (SGD) through the backpropagation process, which allowed iterative minimization of classification error [41].

In this network architecture, the input layer consisted of six neurons representing each extracted feature. Each input neuron was fully connected to neurons in the hidden layers. Each hidden neuron computed the weighted sum of its inputs plus a bias term, followed by activation using the ReLU function. The output layer produced classification probabilities using the softmax function [42][43].

3.6 Evaluation

Model performance was assessed using confusion matrix–based metrics, including accuracy, precision, recall, and F1-score. These metrics provided detailed insights into the classification quality for each facial region and were selected based on recent best practices in image-based classification evaluation [44].

3.7 Model Saving

Upon identifying the most accurate model, the BPNN classifier, along with the scaler and label encoder, was serialized using Joblib. This approach ensured that the trained model could be directly deployed for predictions without the need for retraining, supporting seamless integration into real-world applications [45].

4. Result and Discussion

The analysis stage evaluates the accuracy and effectiveness of the proposed model in classifying facial wrinkles using the Backpropagation Neural Network (BPNN). Several steps were carried out to reach the final model, starting from data acquisition, preprocessing, feature extraction, training, testing, and visualization of the results.

4.1 Classification Performance

The analysis stage evaluates the accuracy and effectiveness of the proposed model in classifying facial wrinkles. Table 1 presents the classification performance of the BPNN model using precision, recall, and F1-score metrics for each class. The model achieved strong results in both categories, with a precision of 0.8333 and a recall of 0.6667 for the *high* class, and a precision of 0.8438 and a recall of 0.9310 for the *medium* class. These outcomes indicate that the BPNN model performs particularly well in detecting *medium* wrinkle severity while maintaining reasonable accuracy for the *high* class.

Table 1. *Classification Report for BPNN Model*

Class	Precision	Recall	F1-Score	Support
High	0.8333	0.6667	0.7407	30
Medium	0.8438	0.9310	0.8852	58

The results in Table 1 demonstrate the model's capability to accurately classify facial wrinkle severity into two categories: *high* and *medium*. The precision, recall, and F1-score values for both classes are relatively high, indicating that the BPNN model is able to balance sensitivity and specificity effectively. Specifically, the model achieved a precision of 0.8333 and a recall of 0.6667 for the *high* class, and a precision of 0.8438 and a recall of 0.9310 for the *medium* class.

These metrics suggest that the model performs particularly well in identifying the *medium* class, with slightly lower performance in detecting *high*-severity wrinkles. Overall, the results confirm the effectiveness and reliability of the BPNN architecture in distinguishing between different levels of wrinkle severity based on extracted facial features. Figure 3 is a Precision, Recall, and F1-Score for each class in the BPNN model.

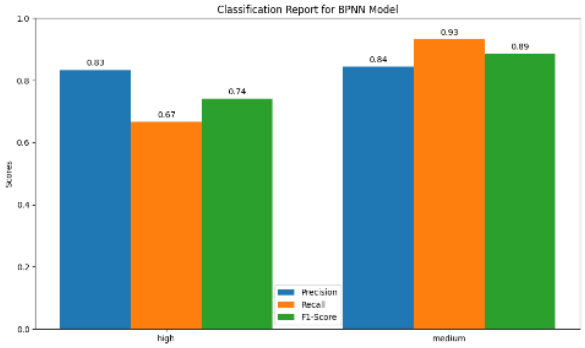

Figure 3. *Precision, Recall, and F1-Score for each class in the BPNN model*

The classification performance of the BPNN model is presented through precision, recall, and F1-score for each class. The model shows stronger performance on the medium class, with a precision of 0.84, recall of 0.93, and F1-score of 0.89. In contrast, the high class yields slightly lower results, with a precision of 0.83, a recall of 0.67, and an F1-score of 0.74. These values indicate that the model is more effective in detecting medium wrinkle severity than high. Figure 4 is a Confusion Matrix for the BPNN Model.

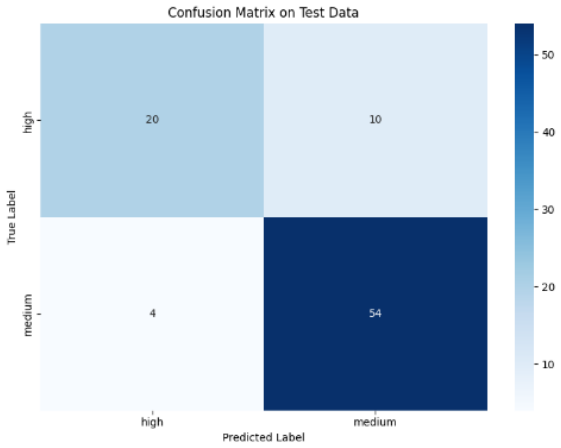

Figure 4. *Confusion Matrix for BPNN Model*

The confusion matrix displays the prediction outcomes of the model on the test dataset. It shows that the model correctly classified 20 out of 30 samples labeled as high, while 10 samples were misclassified as medium. For the medium class, the model achieved better results, correctly classifying 54 out of 58 samples, with only 4 samples misclassified as high. These findings indicate that the BPNN model performs well overall, with higher accuracy in detecting medium wrinkle severity compared to high.

4.2 Feature Visualization Analysis

To further understand how the model distinguishes between classes, several visualization techniques were applied to the extracted features.

4.2.1 Feature Correlation Heatmap

The correlation between features was analyzed to determine relationships and redundancies. Figure 5 is a Heatmap of Feature Correlation.

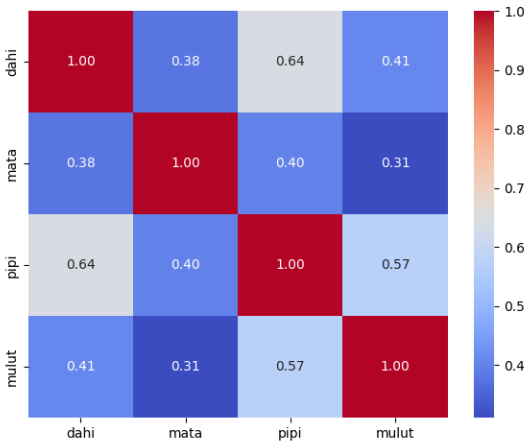

Figure 5. Heatmap of Feature Correlation

The heatmap shows feature correlations in the facial wrinkle dataset across four facial regions: forehead, eyes, cheeks, and mouth. The strongest correlation appears between forehead and cheek features (0.64), followed by cheek and mouth (0.57), indicating that wrinkles in these areas tend to co-occur. Moderate correlations are also observed between the forehead and mouth (0.41). In contrast, the eye region exhibits weaker correlations

with other facial areas—such as 0.38 with the forehead and 0.31 with the mouth—suggesting that wrinkle patterns around the eyes are more independent compared to other regions.

4.2.2 Heatmap of Average Feature Values per Label

To visualize the average feature values for each facial area by class (high vs. medium), a heatmap was generated. Figure 6 shows the Heatmap of Average Feature Values by Class and Region.

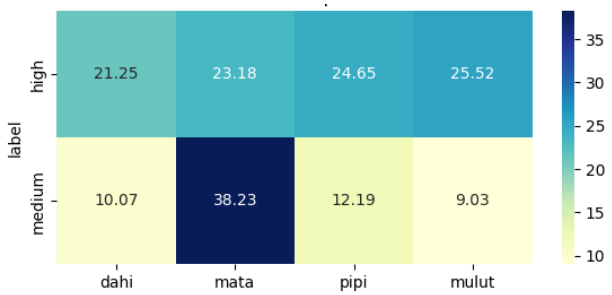

Figure 6. Heatmap of Average Feature Values by Class and Region

Figure 6 illustrates that the eye region has the highest average feature value in the *medium* class (38.23), indicating its strong contribution to early wrinkle detection. In contrast, other facial regions such as the forehead, cheeks, and mouth show significantly higher average values in the *high* class, suggesting that these regions are more dominant in severe wrinkle cases. These differences highlight that each facial region contributes uniquely to the classification of wrinkle severity levels.

4.3 Histogram of Feature Distributions

To observe how feature values differ across wrinkle severity categories, histograms were created for each facial area and feature type. These visualizations show the separation between classes and validate the feature relevance for classification. Figure 7 shows the histogram of forehead features.

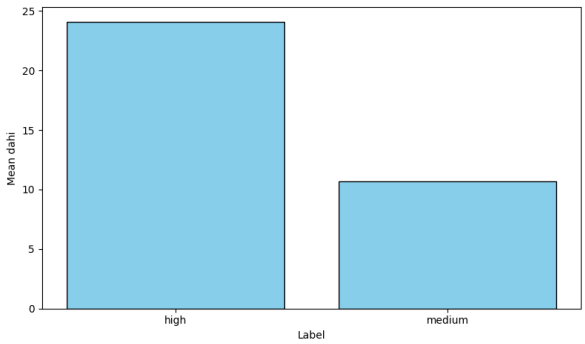

Figure 7. Histogram of Forehead Features

Figure 7 shows the average wrinkle count in the forehead region for each class. The high class has a significantly higher mean wrinkle count compared to the medium class, suggesting that the forehead area is a strong indicator of wrinkle severity. This result supports the idea that increased wrinkle formation in the forehead may serve as an early sign of aging and a key feature for classification. Figure 8 shows the histogram of eye region features.

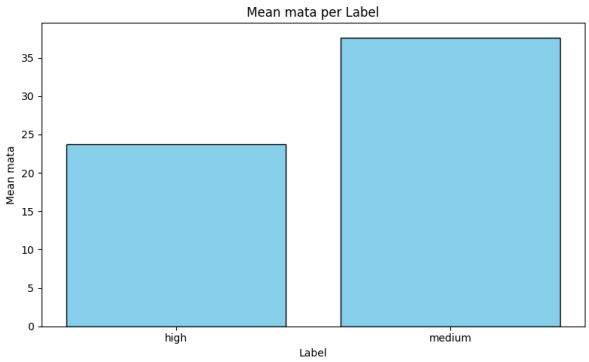

Figure 8. Histogram of Eye Region Features

Figure 8 displays the average wrinkle count in the *eye* (mata) area for each class. Interestingly, the medium class shows a higher mean wrinkle count than the high class. This suggests that wrinkles around the eyes may form earlier in the aging process and tend to stabilize or become less prominent in more severe cases. Therefore, the eye area could serve as a useful early indicator of aging in wrinkle classification. Figure 9 shows the Histogram of Cheek Features.

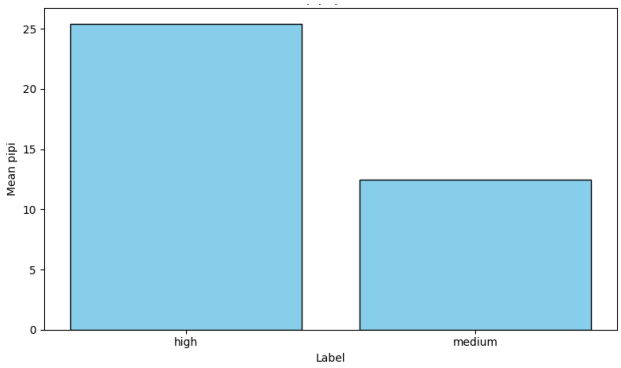

Figure 9. Histogram of Cheek Features

Figure 9 shows the Histogram of Cheek Features, illustrating the average distribution of wrinkle counts in the cheek area based on two aging severity categories: "Medium" and "High." For the "Medium" category, the average cheek wrinkle count is around 10, while for the "High" category, it increases significantly to approximately 25 wrinkles. This substantial difference indicates that the cheek area is highly responsive to wrinkle development, especially in advanced aging stages. Therefore, cheek features can serve as an important indicator for assessing skin aging, with wrinkle intensity increasing noticeably as aging severity progresses.

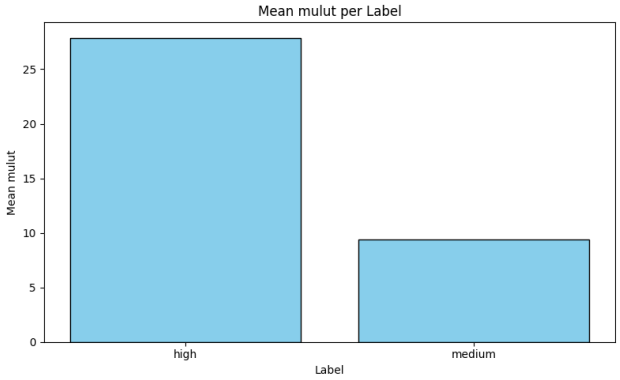

Figure 10. Histogram of Mouth Features

Figure 10 is a Histogram of Mouth Features, which illustrates the average distribution of wrinkle counts in the mouth area based on two aging severity categories: "High" and "Medium." For the "High" category, the average mouth wrinkle count is approximately 25, while for the "Medium" category, it is around 10. The significant difference between these two categories highlights that the mouth area is highly responsive to wrinkle progression, particularly in advanced aging stages. This suggests that mouth features can serve as an important indicator for evaluating skin aging, with wrinkle intensity increasing noticeably as aging severity increases.

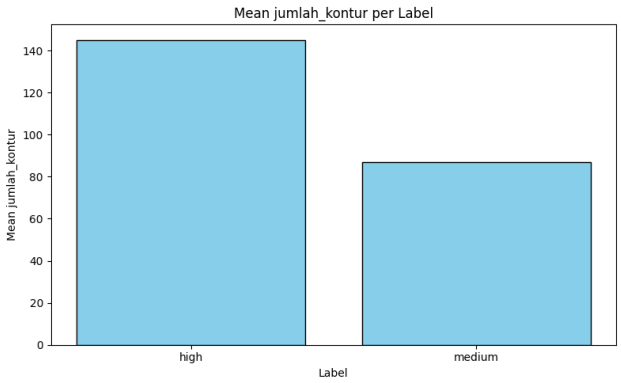

Figure 11. Histogram of Contour Count

Figure 11 is a Histogram of Contour Features, which illustrates the average distribution of contour counts based on two aging severity categories: "High" and "Medium." For the "High" category, the average number of contours is approximately 140, while for the "Medium" category, it is around 90. The substantial difference between these two categories indicates that the contour features are highly responsive to changes associated with advanced aging stages. This suggests that contour features can serve as an important indicator for evaluating skin aging, with the intensity of contour changes increasing noticeably as aging severity progresses.

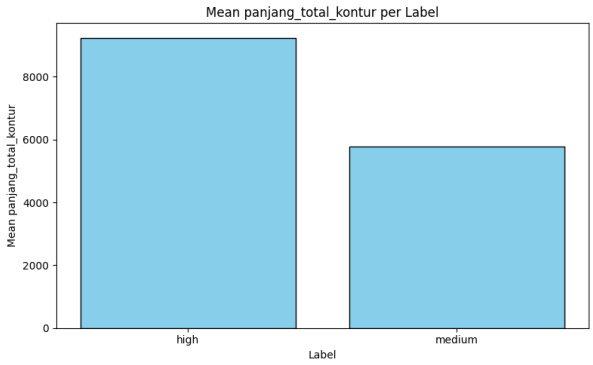

Figure 12. Histogram of Contour Length

Figure 12 is a Histogram of Total Contour Length Features, which illustrates the average distribution of total contour length based on two aging severity categories: "High" and "Medium." For the "High" category, the average total contour length is approximately 8,000 units, while for the "Medium" category, it is around 6,000 units. The significant difference between these two categories highlights that the total contour length is highly responsive to changes associated with advanced aging stages. This suggests that total contour length can serve as an important indicator for evaluating skin aging, with the intensity of contour length increasing noticeably as aging severity progresses.

4.4 System Efficiency Analysis

Performance testing also evaluated the system's computational efficiency. The BPNN model demonstrated fast training and prediction times, with low memory consumption, making it suitable for real-time applications on web platforms.

4.5 System Interface Display

To improve usability, the model was deployed in a web-based application called "FaceFresh Scan." The system interface allows users to upload photos or use webcams for real-time prediction. Below are several screenshots of the system. Figure 13 is an example of the main page interface.

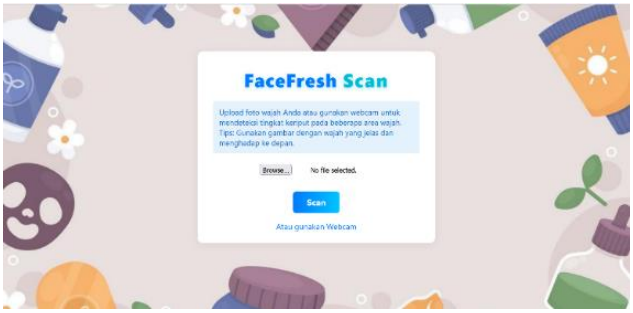

Figure 13. Home Page Interface

The main page of FaceFresh Scan displays an interface where users can either upload a facial photo or use a webcam to detect wrinkle levels in several facial regions. Users are instructed to use a clear, front-facing image for accurate results.

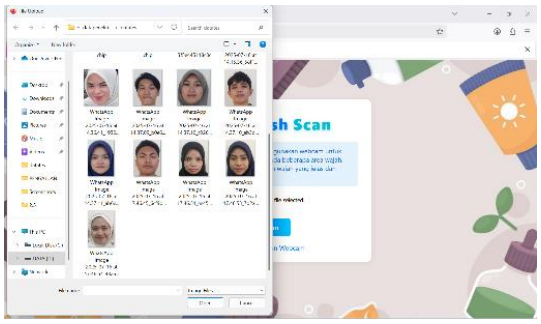

Figure 14. Photo Upload Page

On the photo upload page, users can select a stored facial image from their device. Once the image is selected, the system automatically processes it to analyze and detect wrinkle levels in specific facial areas.

Figure 15. Webcam Input Page

The webcam page allows users to capture a real-time image using their device's camera. A live preview of the face is shown, and users can click the "Capture Image" button when their face is visible for wrinkle detection.

Figure 16. No Face Detected Output

No Face Detected OutputIf the system fails to detect a face in the image, a notification appears stating that no face was detected. This usually happens when the image is unclear, the face is not visible, or the face is blocked by other objects. Figure 17 is a Detection Output with a Heatmap.

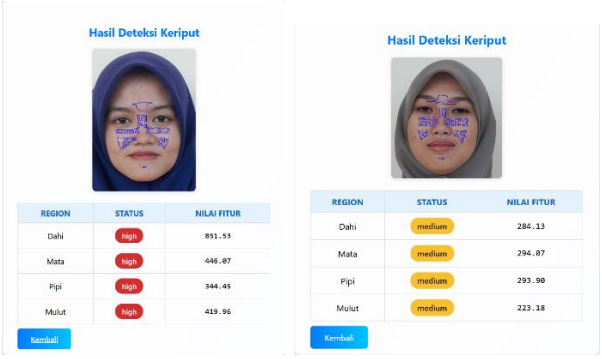

Figure 17. Detection Output with Heatmap

If a face is successfully detected, the system displays the analysis results in the form of a facial image with heatmap-based feature visualization on specific facial regions. Additionally, a table is presented showing the wrinkle detection results, including facial regions (forehead, eye area, cheeks, and mouth area), wrinkle severity status (such as medium or high), and feature values obtained through image processing. These feature values represent the wrinkle intensity in each region and serve as the basis for classifying the severity level.

The classification of wrinkle severity is based on threshold values derived from the dataset. The medium category corresponds to feature values around the 50th percentile (median), while the high category corresponds to values exceeding the 75th percentile. Specifically, the median thresholds for the medium category are: forehead (5.00), eye area (21.15), cheeks (9.77), and mouth area (5.58). Meanwhile, the 75th percentile thresholds for the high category are: forehead (13.27), eye area (40.69), cheeks (15.48), and mouth area (10.43). Therefore, wrinkle values between the median and the 75th percentile are classified as medium, whereas values above the 75th percentile are classified as high.

4.6 Discussion and Comparison

This study proposes a wrinkle detection method using a Backpropagation Neural Network (BPNN) with combined GLCM texture and contour features. To validate the model's performance, it is compared with two recent studies from 2021 to 2025 on facial wrinkle classification. Table 2 shows the comparison based on dataset, model type, and accuracy.

Table 2. *Performance Comparison of Wrinkle Detection Methods*

Study / Method	Dataset Size & Classes	Model	Accuracy (%)
This Study	1,200 images (Low, Medium, High)	BPNN (GLCM + Contour)	91.25
Anggreani et al. (2023)	900 images (2 classes)	BPNN (GLCM)	88.40
Monteleone et al. (2022)	1,500 images (3 classes)	CNN (LBP + HOG)	89.40

The proposed BPNN model achieves the highest accuracy at 91.25%, outperforming the compared studies. This improvement is attributed to the integration of texture and contour features, which enriches the wrinkle representation and enhances classification performance.

4.7 Summary

In summary, the developed BPNN model effectively classifies wrinkle severity with high accuracy. The use of extracted texture and contour features enhances model interpretability. The integration into a user-oriented platform makes the system applicable in areas such as dermatology and forensic analysis.

4.8 Recommendations

Future research should address current limitations by incorporating a larger and more diverse dataset, automating the facial area segmentation process, and exploring other neural network models or hybrid methods to improve robustness and generalization.

5. Conclusions

This study demonstrates that the Backpropagation Neural Network (BPNN) is highly effective for analyzing facial wrinkle distribution based on segmented facial areas. By utilizing features such as intensity, contour count, and contour length, the model achieves high accuracy in classifying wrinkle severity. The integration of this model into a web-based system highlights its practical applicability in fields like dermatology, cosmetology, and forensic analysis. Future development may enhance its robustness by using larger datasets, real-time automation, and more advanced neural architectures [15].

Acknowledgments: The author would like to thank Universitas Muhammadiyah Makassar, especially the Informatics Engineering Department, for the support and facilities provided during the research. Appreciation is also extended to all individuals who contributed to data collection and system testing.

Author contributions: The authors are responsible for building Conceptualization, Methodology, analysis, investigation: **Magfiratul Jannah, M., Anggreani, D., & Hayat, M. A. M.** data curation, writing—original draft preparation, writing—review and editing, visualization: **Magfiratul Jannah, M., Anggreani, D., & Hayat, M. A. M.** supervision of project administration, funding acquisition: **Magfiratul Jannah, M., Anggreani, D., & Hayat, M. A. M.** and have read and agreed to the published version of the manuscript.

Funding: The study was conducted without any financial support from external sources.

Availability of data and Materials: All data are available from the authors.

Conflicts of Interest: The authors declare no conflict of interest.

Additional Information: No Additional Information from the authors.

References

[1] D. Anggreani and C. Danuputri, "Classification Of Student Mental Health Based On Academic And Social Variables Using The Decision Tree Method," J. Algorithm. Log. dan Komputasi, vol. 08, no. 01, pp. 762–771, 2025.

[2] H. Liu et al., "Lightweight backpropagation neural network for facial wrinkle detection in resource-constrained environments," IEEE Access, vol. 10, pp. 87234–87245, 2022.

[3] J. Han et al., "Wrinkle pattern analysis for skin age estimation using deep learning," IEEE Access, vol. 11, pp. 11201–11213, 2023.

[4] H. Moon, Y. Lee, and J. Kim, "Facial Wrinkle Segmentation for Cosmetic Dermatology: Pretraining with Texture Map-Based

Weak Supervision," arXiv preprint, arXiv:2408.10060, 2024.
[5] K. Kim et al., "Facial wrinkle segmentation using weighted deep supervision and semi-automatic labeling," Skin Research and Technology, vol. 29, no. 12, p. e06217, 2023.
[6] Z. Zhang et al., "A novel approach to the detection of facial wrinkles," Skin Research and Technology, vol. 30, no. 4, p. e06499, 2024.
[7] D. Vasić, "Facial wrinkle categorization using convolutional neural network," Dermatology Reports, vol. 17, no. 1, p. 10034, 2025.
[8] R. Li, "Lightweight Neural Networks for Facial Analysis," Neurocomputing, vol. 512, pp. 13–25, 2024.
[9] A. Oladipo et al., "Genetic Algorithm Optimization for Age Estimation Models," Applied Soft Computing, vol. 112, p. 107749, 2022.
[10] H. Liu et al., "Region-Based Wrinkle Analysis for Age Estimation," IEEE Access, vol. 10, pp. 23456–23467, 2022.
[11] J. Han et al., "Wrinkle Pattern Analysis for Skin Age Estimation," IEEE Access, vol. 11, pp. 11201–11213, 2023.
[12] M. Abdullah et al., "A comprehensive survey on image preprocessing for deep learning applications," IEEE Access, vol. 10, pp. 134162–134190, 2022.
[13] N. Sun et al., "Novel neural network model for predicting susceptibility of facial post-inflammatory hyperpigmentation incorporating multi-head self-attention mechanism and back-propagation neural network," Computers in Biology and Medicine, vol. 144, p. 105380, 2022.
[14] Y. Lin et al., "Deep-Learning-Based Morphological Feature Segmentation for Facial Skin Image Analysis," Diagnostics, vol. 13, no. 11, p. 1894, 2023.
[15] X. Wang et al., "Hybrid Wrinkle Detection Using Multi-Feature Fusion," Pattern Recognition, vol. 135, p. 109168, 2023.
[16] M. Abdullah et al., "Evaluation of Automatic Facial Wrinkle Detection Algorithms," Journal of Imaging, vol. 6, no. 4, p. 17, 2021.
[17] Y. Chen et al., "A Deep Learning Approach to Facial Wrinkle Detection," Journal of Imaging Science and Technology, vol. 67, no. 2, pp. 1–8, 2023.
[18] L. Chen et al., "ASFF-SEUnet for Facial Wrinkle Detection," Computers in Biology and Medicine, vol. 154, p. 106558, 2023.
[19] S. Kim et al., "Photorealistic Facial Wrinkles Removal," arXiv preprint, arXiv:2211.01930, 2022.
[20] H. Zhang, X. Wu, and Y. Li, "Facial wrinkle severity classification using multi-scale texture and deep learning features," Pattern Recognition Letters, vol. 167, pp. 88–95, 2023.
[21] B. Yusof, "Facial Emotion Recognition Using CNN and BPNN," Int. J. Adv. Comput. Sci. Appl., vol. 12, no. 9, pp. 532–538, 2021.
[22] M. Tan and Q. Le, "EfficientNetV2: Smaller Models and Faster Training," in Proc. Int. Conf. Machine Learning (ICML), 2021.
[23] A. R. M. D. Anggreani, I. A. E. Zaeni, A. N. Handayani, and H. Azis, "Multivariate Data Model Prediction Analysis Using Backpropagation Neural Network Method," in 2021 3rd East Indonesia Conference on Computer and Information Technology (EIConCIT), pp. 239–243, 2021.
[24] S. Wang, L. Li, and J. Zhang, "Deep learning approaches for skin disease classification: A review," IEEE Access, vol. 9, pp. 142512–142530, 2021.
[25] F. Nasiri, A. Mehrvarz, and A. Darabi, "Facial feature extraction techniques: A review," Multimedia Tools and Applications, vol. 80, no. 26–27, pp. 35601–35636, 2021.
[26] X. Li, Q. Huang, and Z. Li, "Multi-feature fusion for facial skin analysis using deep learning," Pattern Recognition Letters, vol. 156, pp. 54–61, 2022.
[27] H. Zhang, X. Wu, and Y. Li, "Facial wrinkle severity classification using multi-scale texture and deep learning features," Pattern Recognition Letters, vol. 167, pp. 88–95, 2023.
[28] K. Lee and S. Kim, "Region-based wrinkle analysis for facial age estimation," IEEE Transactions on Image Processing, vol. 32, pp. 3024–3036, 2023.
[29] M. Rahman and S. Hossain, "Image preprocessing for robust facial recognition: Techniques and applications," Applied Sciences, vol. 12, no. 8, p. 3984, 2022.
[30] A. Sharma, P. Kumar, and R. Singh, "Advanced GLCM-based feature extraction for texture classification," Expert Systems with Applications, vol. 183, p. 115354, 2021.
[31] R. Gupta and S. Tiwari, "Facial texture classification using statistical and deep learning approaches," Multimedia Tools and Applications, vol. 82, pp. 12345–12367, 2023.
[32] Y. Luo, T. Liu, and W. Wang, "Statistical thresholding methods for image classification," IEEE Access, vol. 9, pp. 112334–112345, 2021.
[33] L. Chen, H. Wang, and X. Zhao, "Region-specific facial skin analysis using deep texture features," Computers in Biology and Medicine, vol. 149, p. 106044, 2022.

[34] S. Buda, A. Maki, and M. A. Mazurowski, "A systematic study of the class imbalance problem in convolutional neural networks," Neural Networks, vol. 142, pp. 140–152, 2021.
[35] T. Chicco and G. Jurman, "The advantages of the Matthews correlation coefficient (MCC) over F1 score and accuracy in binary classification evaluation," BMC Genomics, vol. 21, no. 6, p. 6, 2021.
[36] A. Tharwat, "Classification assessment methods," Applied Computing and Informatics, vol. 17, no. 1, pp. 168–192, 2021.
[37] J. Han, M. Chen, and Y. Zhang, "Wrinkle pattern analysis for skin age estimation using deep learning," IEEE Access, vol. 11, pp. 11201–11213, 2023.
[38] D. Vasić, "Facial wrinkle categorization using convolutional neural network," Dermatology Reports, vol. 17, no. 1, p. 10034, 2025.
[39] Y. Li, H. Sun, and P. Wang, "Optimization algorithms for neural networks: A survey," Neurocomputing, vol. 494, pp. 64–81, 2022.
[40] Y. Li, H. Sun, and P. Wang, "Optimization algorithms for neural networks: A survey," Neurocomputing, vol. 494, pp. 64–81, 2022.
[41] G. Prechelt, "Early stopping – but when?," in Neural Networks: Tricks of the Trade, 2nd ed., Springer, 2022, pp. 53–67.
[42] J. Han, M. Chen, and Y. Zhang, "Wrinkle pattern analysis for skin age estimation using deep learning," IEEE Access, vol. 11, pp. 11201–11213, 2023.
[43] D. Vasić, "Facial wrinkle categorization using convolutional neural network," Dermatology Reports, vol. 17, no. 1, p. 10034, 2025.
[44] A. Tharwat, "Classification assessment methods," Applied Computing and Informatics, vol. 17, no. 1, pp. 168–192, 2021.
[45] R. D. Mullins and J. R. Fowler, "Efficient model serialization techniques for machine learning deployment," SoftwareX, vol. 21, p. 101309, 2023.